Modeling the Broad-Band Emission from the Gamma-Ray Emitting Narrow-Line Seyfert-1 Galaxies 1H 0323+342 and B2 0954+25A

Maialen Arrieta-Lobo*, Catherine Boisson and Andreas Zech

Laboratoire Univers et Theories, Observatoire de Paris, CNRS, Université Paris-Diderot, PSL Research University, Meudon, France

Prior to the Fermi-LAT era, only two classes of Active Galactic Nuclei (AGN) were thought to harbor relativistic jets that radiate up to gamma-ray energies: blazars and radio galaxies. The detection of variable gamma-ray emission from Narrow Line Seyfert 1 (NLSy1) galaxies has put them on the spotlight as a new class of gamma-ray emitting AGN. In this respect, gamma-ray emitting NLSy1s seem to be situated between blazars (dominated by non-thermal emission) and Seyferts (accretion disc dominated). In this work, we model the Spectral Energy Distribution (SED) of two gamma-loud NLSy1s, 1H 0323+342 and B2 0954+25A, during quiescent and flaring episodes via a multi-component radiative model that features a relativistic jet and external photon fields from the torus, disc, corona and Broad Line Region (BLR). We find that the interpretation of the high-energy emission of jetted NLSy1s requires taking into account Inverse Compton emission from particles in the relativistic jet that interact with external photon fields. Minimal changes are applied to the model parameters to transition from average to flaring states. In this scenario, the observed variability is explained mainly by means of changes in the jet density and Doppler factor.

Keywords: AGN, quasar, NLSy1, blazar, gamma-ray, modeling, 1H 0323+342, B2 0954+25A

1. INTRODUCTION

Blazars are AGN whose relativistic jet is pointing closely toward the Earth, which results in strong relativistic beaming of the observed radiation (a.k.a. Doppler boosting). This type of AGN can be further classified into Flat Spectrum Radio Quasars (FSRQs) and BL Lac objects, the main difference being the presence of features in the optical spectra of the former, and lack thereof in the case of the latter. The SED of both blazar subtypes spans a frequency range over 20 orders of magnitude in frequency, from radio frequencies up to gamma-rays. However, while the BL Lac subclass presents a SED with two clearly defined bumps, namely the synchrotron and the Inverse Compton (IC) bumps that can be accurately described by a simple one-zone leptonic Synchrotron Self-Compton (SSC) emission model, the FSRQ subtype features a more complex emission spectrum that requires radiation from external photon fields such as the accretion disc or the dusty torus to be accounted for (see e.g., Ghisellini and Tavecchio, 2009). The unexpected detection of gamma-ray emission from a particular type of Seyfert 1 galaxies, NLSy1s, who were not expected to harbor relativistic jets that could create such high-energy emission, has originated a new gamma-loud class of AGN. So far, 10 gamma-ray emitting NLSy1 galaxies have been detected with the Large Area Telescope onboard the Fermi satellite (see for instance, the 3FGL catalog Acero et al., 2015).

The fact that this new type of gamma-loud AGN features both blazar- and Seyfert-like characteristics could bring us closer to a better understanding of AGN unification theories. In fact, their broad-band SED resembles the one of FSRQs, since emission from features other than the relativistic jet are observed. Here, we consider two different states, based on the variability of the gamma-ray flux, for two of the NLSy1s detected with Fermi, 1H 0323+342 and B2 0954+25A, and apply a multi-component radiative model that considers both the emission from the relativistic jet and the external photon fields (torus, disc, corona, and BLR). Further details and references are given in section 2. The main difference between our model and previous models (e.g., Calderone et al., 2012; Paliya et al., 2014) is that we consider several emission lines from the BLR (Cerruti et al., 2013b) and we describe different states of the same source by applying minimal changes to the jet parameters of the model. In the following sections, we present the multi-component model (section 2), along with the application to two datasets of each selected source (section 3) to conclude with a brief discussion and outlook (section 4). Throughout this work, a ΛCDM cosmology is assumed with $H_0 = 70$ km s^{-1} Mpc^{-1}, $\Omega_m = 0.3$ and $\Omega_\Lambda = 0.7$.

2. THE MULTI-COMPONENT CODE

In the pure one-zone SSC model, radiation is produced in a single zone of the jet approximated as a sphere of radius R_{src} (a.k.a. the blob) with a tangled magnetic field B which moves through the jet with bulk Lorentz factor Γ oriented at a small viewing angle θ (see Katarzyński et al., 2001 for further details). This description implies that the photons up to X-ray energies forming the first broad bump observed in the SED of BL Lac type blazars are produced by a population of relativistic electrons via synchrotron radiation. These synchrotron photons are then IC scattered by the same population of electrons up to gamma-ray energies, creating the second broad bump featured in the SED.

Although this simple SSC model approximation quite accurately describes the SED of BL Lac type objects, it is not sufficient to account for the radiation observed in other gamma-loud AGN classes, e.g., FSRQs or certain NLSy1 galaxies. Thus, in addition to the synchrotron and Inverse Compton radiation from the blob-in-jet scenario, it is necessary to add external photon-field contributions. Our multi-component code is based on a stationary homogeneous one-zone SSC model with additional external photon fields from the dusty torus, the accretion disc, the X-ray corona and the Broad-Line Region (BLR) as illustrated in **Figure 1**, and based on Cerruti et al. (2013b), Dermer and Menon (2009), Donea and Protheroe (2003), Finke et al. (2008), Finke and Dermer (2010), and Finke (2016).

The accretion disc is described as a multi-temperature black body (Dermer and Menon, 2009), while the torus is a simple black body (Dermer and Menon, 2009). The X-ray corona is treated as a simple power law function with an exponential cut-off at around 150 keV (Ghisellini et al., 2009). Accretion disc and corona photons will ionize the BLR, which is considered as a spherical shell of width ΔR expanding between an inner and

an outer radius ($\Delta R \ll R_{in}, R_{out}$). The density of the BLR has a power law shape within ΔR, with an index ξ fixed to $\xi = -2$ that implies that most of the ionization takes place close to the inner edge of the BLR (see Dermer and Menon, 2009; Finke and Dermer, 2010 for a detailed explanation). Thus, the BLR will emit a spectrum of monochromatic emission lines (see Cerruti et al., 2013b for more details). The torus, the corona and the BLR are scaled to the disc luminosity through the covering factors τ_{IR}, τ_X and τ_{BLR} respectively that are considered as free parameters (see **Figure 1**). The external photon fields are comptonized when they encounter the relativistic electrons from the blob (Dermer and Menon, 2009). The luminosity of the EIC components is strongly dependent on the distance between the black hole and the blob within the jet. Note that the radius of the torus and the radius of the BLR scale with the disc luminosity, which depends on the black hole mass M_{BH} and the radiative efficiency (see for instance Ghisellini and Tavecchio, 2009), reducing the number of free parameters of the model.

3. APPLICATION

In the following section, we present some of the main characteristics of the gamma-loud NLSy1s to which we applied our multi-component model, namely 1H0323+342 and B2 0954+25A. For the modeling, two different datasets are considered for each source: a quiescent/average dataset and a flaring state dataset w.r.t. gamma-ray emission seen by Fermi. The parameter sets that best describe the data along with a brief discussion on the model interpretation are then provided.
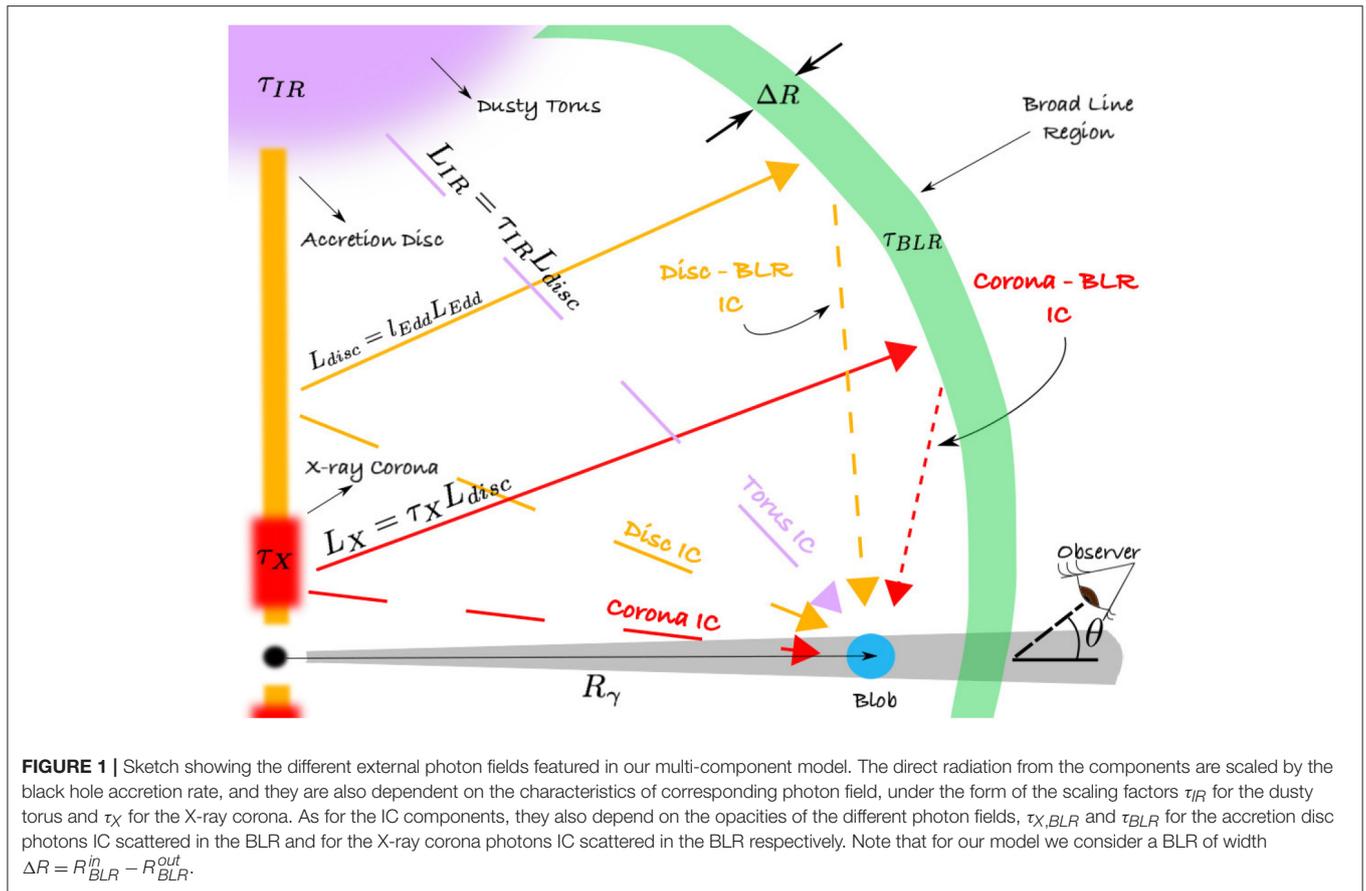
3.1. 1H 0323+342

1H 0323+342 is the closest gamma-loud NLSy1 known, located at $z = 0.063$. One of its most interesting features is its frequent variability both in X-rays and gamma-rays which, although often uncorrelated, sometimes presents hints of correlation (Paliya et al., 2014). The black hole mass is $M_{BH} = 2 \times 10^7 M_\odot$ (Landt et al., 2017), and the viewing angle was estimated to be $\theta \sim 4°$ $- 13°$ in Fuhrmann et al. (2016). For our models, we arbitrarily fixed $\theta = 5°$.

3.1.1. Data Sample and Analysis

Average Swift XRT and UVOT data from observations taken in September 2013 and December 2014 with NuSTAR data from March 2014 (see Landt et al., 2017 for further details) and Fermi data from the low state in Paliya et al. (2014) are considered as the quiescent state of the source, depicted in light green in **Figure 2**. Simultaneous Fermi-LAT from August 27th 2013 to August 31st 2013 and Swift UVOT and XRT data from Paliya et al. (2014) are taken into account for the flaring state (orange data points and bow-tie in **Figure 2**).

3.1.2. Modeling the SED

Top and bottom panels in **Figure 2** present the quiescent state and high state model results for 1H 0323+342 respectively. The corresponding model parameters are shown in **Table 1**. We are trying to model the two states with a minimum of parameter changes, assuming that only the compact jet component varies.

FIGURE 1 | Sketch showing the different external photon fields featured in our multi-component model. The direct radiation from the components are scaled by the black hole accretion rate, and they are also dependent on the characteristics of corresponding photon field, under the form of the scaling factors τ_{IR} for the dusty torus and τ_X for the X-ray corona. As for the IC components, they also depend on the opacities of the different photon fields, $\tau_{X,BLR}$ and τ_{BLR} for the accretion disc photons IC scattered in the BLR and for the X-ray corona photons IC scattered in the BLR respectively. Note that for our model we consider a BLR of width $\Delta R = R_{BLR}^{in} - R_{BLR}^{out}$.

At sub-millimeter and infrared frequencies, the relativistic jet is necessary to account for the radiation from the source both in the quiescent and high states. The presence of the accretion disc is a major contribution in this source at UV/optical wavelengths. During flaring states the larger contribution from the jet in combination with direct emission from the torus and disc gives a good description of the observed radiation. The dip at optical frequencies in the quiescent state model is due to the steep slope of the Fermi-LAT data that forces the index of the particle distribution after the energy break to be steep too. However, we need to remark that these are not simultaneous data.

As for X-rays, in the quiescent state the hard emission is well explained by the X-ray corona component, while a larger contribution from the jet SSC radiation by means of a larger Doppler factor ($\delta = 11$ vs. $\delta = 9$ for the quiescent state) is necessary to reach the observed hard X-ray flux levels in the flaring state. At gamma-ray frequencies, the EIC emission from the jet explains the observed emission in both the quiescent and the high state: gamma-rays are attributed to the BLR emission lines comptonized by the electrons within the relativistic blob, with a disc EIC component bridging the X-ray and gamma-ray radiation in both states. The change in the slope of the gamma-ray Fermi-LAT spectrum between both states requires a harder electron distribution slope n_2 after the break energy γ_b value in the flare state, a hint of a "harder when brighter" trend. The difference in gamma-ray flux levels between both states is

accounted for by the larger Doppler factor of the flare and higher particle density.

The flaring state features a larger particle density w.r.t. the quiescent state. The magnetic field also remains the same between the two states. In this scenario, flaring states seem to occur when a newly expelled blob with a larger Doppler factor goes through a stationary shock within the jet.

Note that to reduce the number of free parameters from our model, we assume that neither the torus, nor the accretion disc not the BLR change during different states of the source. Both quiescent and flaring state models are relatively close to equipartition between the electron distribution kinematic energy density u_e and the magnetic field energy density u_b.

The fact that lowest-energy radio data are not well described by our model is caused by the synchrotron self-absorption of the electron population. Radio data are usually attributed to an extended jet component (Katarzyński et al., 2008; Lenain et al., 2008). Such a component is not considered in our model, but could be added.

3.2. B2 0954+25A

With a redshift of $z = 0.7$, B2 0954+25A is a more distant source than 1H0323+342. Calderone et al. (2012) give a black hole mass of $M_{BH} = 1.5 \times 10^8 \, M_\odot$, and consider a viewing angle of $\theta = 3°$. As documented in the same paper, only a single flare is observed in gamma-ray frequencies during the first half
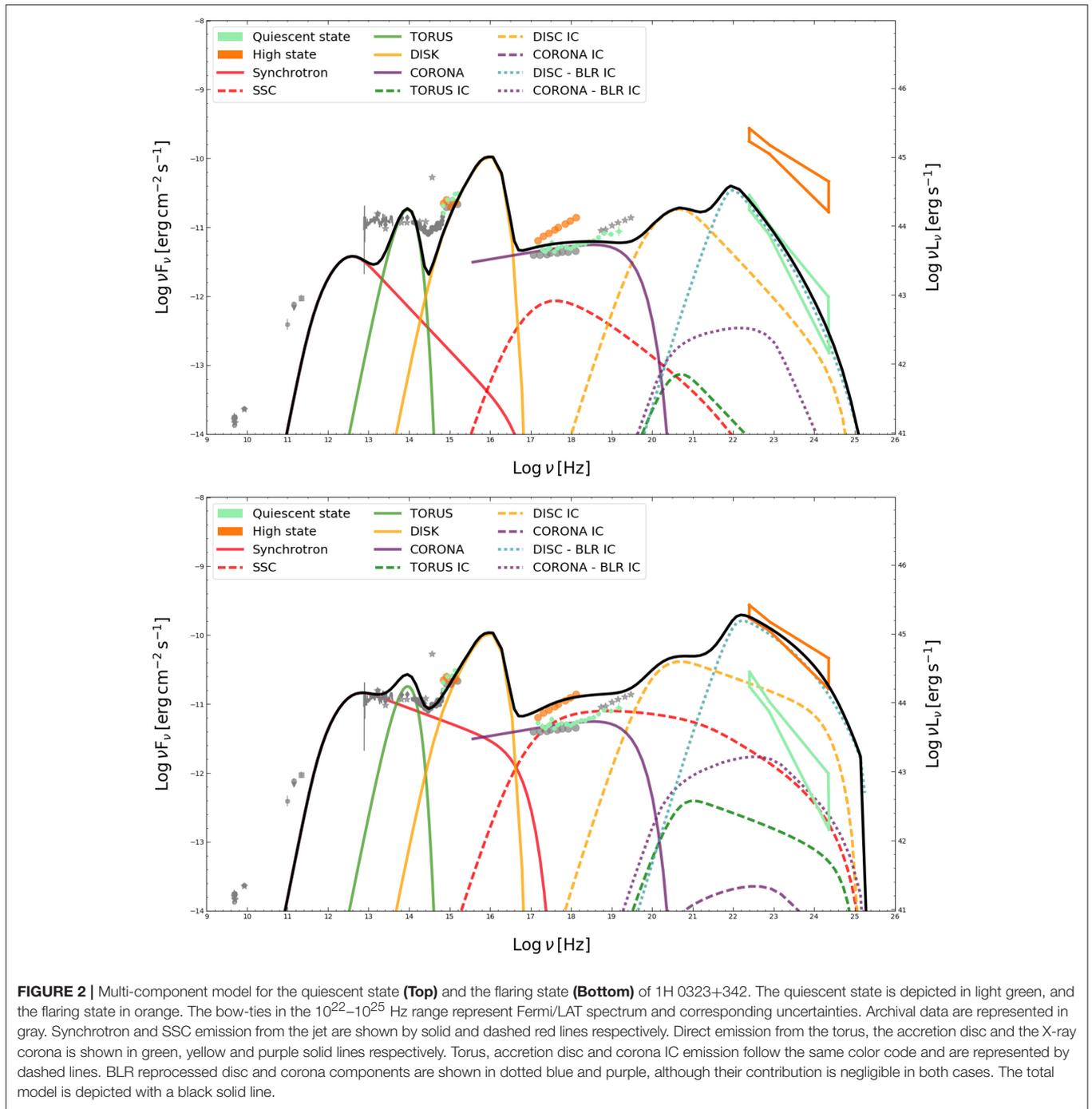
FIGURE 2 | Multi-component model for the quiescent state **(Top)** and the flaring state **(Bottom)** of 1H 0323+342. The quiescent state is depicted in light green, and the flaring state in orange. The bow-ties in the 10^{22}–10^{25} Hz range represent Fermi/LAT spectrum and corresponding uncertainties. Archival data are represented in gray. Synchrotron and SSC emission from the jet are shown by solid and dashed red lines respectively. Direct emission from the torus, the accretion disc and the X-ray corona is shown in green, yellow and purple solid lines respectively. Torus, accretion disc and corona IC emission follow the same color code and are represented by dashed lines. BLR reprocessed disc and corona components are shown in dotted blue and purple, although their contribution is negligible in both cases. The total model is depicted with a black solid line.

of 2010, while the source is quite variable in X-rays. Another interesting fact is that Calderone et al. (2012) propose this source to be a transition object between FSRQs and gamma-loud NLSy1s.

3.2.1. Data Sample and Analysis

To construct the average state, we consider archival Chandra data from 2009 from Calderone et al. (2012) along with long-term averaged (3FGL, 48 months of observations) Fermi-LAT

data (Acero et al., 2015). For the flaring state, we analyzed Fermi-LAT data from the flaring period of the source, i.e., Jan 2010–Jul 2010, and considered them along with Swift XRT and UVOT data from the X-ray flaring period in June 2007. Although there was a contemporary Swift observation taken on June 15, 2010, the statistics are poor due to short exposure time and no good-quality spectrum can be extracted. Given that the count rates between both observations are compatible, we consider the observation from June 2007 for modeling purposes,

TABLE 1 | Model parameters for 1H 0323+342 and B2 0954+25A.

	1H 0323+342		B2 0954+25A	
	Quiescent	**Flare**	**Average**	**Flare**
δ	9	11	13	15
K [1/cm^3]	6.5×10^6	8×10^6	8×10^6	1.3×10^7
R_{src} [cm]	1.15×10^{15}	1.15×10^{15}	4.97×10^{15}	4.97×10^{15}
B [G]	2.6	2.6	2.0	2.0
$n1$	2.2	2.2	2.6	2.7
$n2$	4.2	3.4	3.4	3.4
R_γ [R_G]	3×10^3	3×10^3	3×10^3	3×10^3
l_{Edd}	~ 0.76		~ 0.66	
$\dot{m}$ [$M_\odot$ yr^{-1}]	~ 0.43		~ 2.19	
L_{Disc} [erg s^{-1}]	2×10^{45}		1.13×10^{46}	
u_e/u_b	5.66	9.63	2.7	2.04
n_e [1/cm^3]	1.85×10^6	3.16×10^6	2.87×10^6	2.54×10^6

All the quantities are input parameters to the model except for the last four quantities i.e., $\dot{m}$, L_{Disc}, u_e/u_B and n_e which are derived from the input parameters.

since it is the only Swift observation for which the source was significantly detected. As for 1H0323+342, the average state is depicted in light green, whereas the flare is plotted in orange.

3.2.2. Modeling the SED

Figure 3 shows the multi-component model results for B2 0954+25A in the average and flaring state (top and bottom panels respectively). We follow the same approach as for 1H 0323+342.

In the case of this source, the non-simultaneous infrared and sub-mm emission are underestimated by the synchrotron radiation from the relativistic jet in the average state. Similar to 1H 0323+342, radio data of B2 0954+25A are not well described by our model due to the synchrotron self-absorption of the electron population.

Although less prominent than for 1H0323+342, the presence of the accretion disc is also important in this source at optical/UV frequencies. Unlike for 1H0323+342, the hard X-ray emission is well explained simply by the SSC contribution from the jet both for the average and flaring state. The presence of a X-ray corona is not necessary in this scenario. The jet is necessary to explain gamma-ray emission in both states via inverse comptonization of external photons. In this respect, in both states the gamma emission is attributed to a combination of disc and BLR IC components. No change of the gamma-ray slope is observed between the two states, so the indexes of the electron energy distribution remain unchanged in the case of B2 0954+25A.

Similar to 1H 0323+342, the Doppler factor is higher during the flaring state, while the blob remains at the same position. The blob density remains approximately the same between both states, but there is a small change in the electron spectrum though. No increase of the magnetic field is required from the quiescent to the flaring state, since the only major change is the luminosity of the IC component, which can be well described

by the increase in the electron distribution normalization K and Doppler factor. These variations provide the larger contribution of inverse comptonized external photon fields that is necessary to model the higher fluxes during the flare. Finally, both average state and flaring state solutions are close to equipartition.

4. DISCUSSION AND OUTLOOK

Our multi-component radiative model describes the SED of the two NLSy1s presented here, both in the flaring and quiescent/average states. For both 1H 0323+342 and B2 0954+25A, the gamma-ray radiation is explained by a combination of EIC emission from jet electrons on the photon field from the accretion disc and (dominantly) the BLR. The fact that we model these sources with the same model that is usually applied to FSRQs underlines the similarities between both types of objects.

For each source, the characteristics of the external photon fields are kept constant between different states, to reduce the number of free parameters of the model. All variations are explained by changes in the electron population in the compact relativistic jet.

The transition from quiescent/average to flaring states in both sources is accounted for by a more relativistic flare, i.e., larger Doppler factors, and higher particle densities for 1H 0323+342 while the density is approximately constant for B2 0954+25A. The indexes of the particle energy distribution also vary due to a hardening/flattening of the gamma-ray spectrum. Infrared and sub-mm data are underestimated in the case of B2 0954+25A. This is also the case for the quiescent state of 1H 0323+342, and somewhat less for its flaring state. This might be a hint of the presence of an extended jet in these objects, although data are not simultaneous.

Comparing the present work to previous existing models for the two sources presented here, the scenario in which we model the sources is similar as far as the origin of the external Compton dominance is concerned: in their respective models for 2 states of 1H 0323+342 and one state of B2 0954+25A, Paliya et al. (2014) and Calderone et al. (2012) also describe the high energy emission from the source via the re-emission of disc and BLR photons. The disc luminosities they feature are similar to ours. However, in our scenario the SSC emission is necessary to account for X-ray emission except for the quiescent state of 1H 0323+342.

Due to the large number of free parameters of the model, this type of model is necessarily degenerate. For the simpler SSC model scenario, there are methods to explore the parameter space (Cerruti et al., 2013a), but for more complex EC models like the one we present, this is not the case yet. Our approach is a test for the hypothesis that this type of source can be modeled by this scenario. This is a standard practice for blazar-type source modeling.

Finally, we want to remark that, although solutions dominated by disc and BLR radiation at high energies are presented in this proceeding, models in which the inverse Compton component at high energies is explained mostly by comptonized dusty
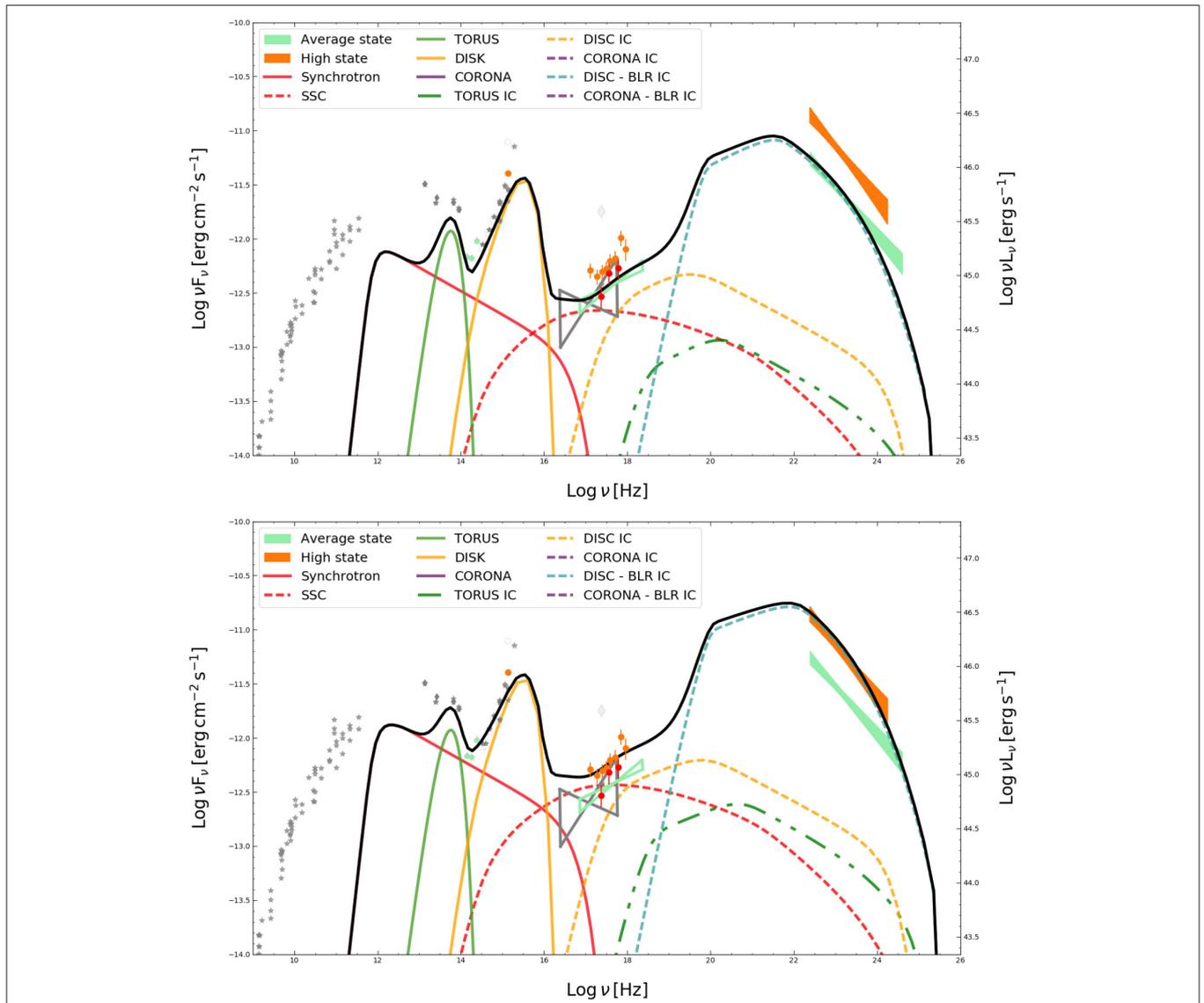
FIGURE 3 | Multi-component model for the average state **(Top)** and the high state **(Bottom)** of B2 0954+25A. The quiescent state is depicted in light green, and the flaring state in orange. The bow-ties in the 10^{22}–10^{25} Hz range represent Fermi/LAT spectrum and corresponding uncertainties. Archival data are represented in gray. Synchrotron and SSC emission from the jet are shown by solid and dashed red lines respectively. Direct emission from the torus and the accretion disc is shown in green and yellow solid lines respectively. Torus and accretion disc IC emission follow the same color code and are represented by dashed lines. The BLR reprocessed disc photon component is shown in dotted blue. Note that there is no presence of the X-ray corona in this scenario. The total model is depicted with a black solid line.

torus radiation can account for NLSy1 SEDs. One of the main differences w.r.t. the disc-dominated scenario is the position of the gamma-ray emitting region: while for the solutions presented here the blob is located well below the BLR, for dust-dominated scenarios the blob is at the outer edge of the BLR where the ionization by the disc photons is at its minimum. Thus, the contribution from the disc and BLR components is minor w.r.t. that of the torus. Furthermore, the dust-dominated scenario requires much larger electron distribution break energies, which means a larger contribution from low-energy electrons that yields solutions that are less absorbed at synchrotron frequencies, such that the synchrotron emission from the blob might account for radio data.

AUTHOR CONTRIBUTIONS

All authors listed, have made substantial, direct and intellectual contribution to the work, and approved it for publication.

FUNDING

ACKNOWLEDGMENTS

REFERENCES

Acero, F., Ackermann, M., Ajello, M., Albert, A., Atwood, W. B., Axelsson, M., et al. (2015). Fermi large area telescope third source catalog. *Astrophys. J. Suppl.* 218:23. doi: 10.1088/0067-0049/218/2/23

Calderone, G., Ghisellini, G., Colpi, M., and Dotti, M. (2012). B2 0954+25A: a typical Fermi blazar or a γ-ray loud Narrow Line Seyfert 1. *Month. Notices R. Astron. Soc.* 424, 3081–3093. doi: 10.1111/j.1365-2966.2012.21456.x

Cerruti, M., Boisson, C., and Zech, A. (2013a). Constraining the parameter space of the one-zone synchrotron-self-Compton model for GeV-TeV detected BL Lacertae objects. *Astron. Astrophys.* 558:A47. doi: 10.1051/0004-6361/201220963

Cerruti, M., Dermer, C. D., Lott, B., Boisson, C., and Zech, A. (2013b). Gamma-ray blazars near equipartition and the origin of the gev spectral break in 3c 454.3. *Astrophys. J. Lett.* 771:L4. doi: 10.1088/2041-8205/771/1/L4

Dermer, C. D., and Menon, G. (2009). *High Energy Radiation from Black Holes: Gamma Rays, Cosmic Rays, and Neutrinos.* Princeton, NJ: Princeton University Press.

Donea, A.-C., and Protheroe, R. J. (2003). Radiation fields of disk, BLR and torus in quasars and blazars: implications for /γ-ray absorption. *Astropart. Phys.* 18, 377–393. doi: 10.1016/S0927-6505(02)00155-X

Finke, J. D. (2016). External compton scattering in blazar jets and the location of the gamma-ray emitting region. *Astrophys. J.* 830:94. doi: 10.3847/0004-637X/830/2/94

Finke, J. D., and Dermer, C. D. (2010). On the break in the fermi-large area telescope spectrum of 3C 454.3. *Astrophys. J. Lett.* 714, L303–L307. doi: 10.1088/2041-8205/714/2/L303

Finke, J. D., Dermer, C. D., and Böttcher, M. (2008). Synchrotron self-compton analysis of TeV X-ray-selected BL lacertae objects. *Astrophys. J.* 686, 181–194. doi: 10.1086/590900

Fuhrmann, L., Karamanavis, V., Komossa, S., Angelakis, E., Krichbaum, T. P., Schulz, R., et al. (2016). Inner jet kinematics and the viewing angle towards the γ-ray narrow-line Seyfert 1 galaxy 1H 0323+342. *Res. Astron. Astrophys.* 16:176. doi: 10.1088/1674-4527/16/11/176

Ghisellini, G., and Tavecchio, F. (2009). Canonical high-power blazars. *Month. Notices R. Astron. Soc.* 397, 985–1002. doi: 10.1111/j.1365-2966.2009.15007.x

Ghisellini, G., Tavecchio, F., and Ghirlanda, G. (2009). Jet and accretion power in the most powerful Fermi blazars. *Month. Notices R. Astron. Soc.* 399, 2041–2054. doi: 10.1111/j.1365-2966.2009.15397.x

Katarzyński, K., Lenain, J.-P., Zech, A., Boisson, C., and Sol, H. (2008). Modelling rapid TeV variability of PKS2155-304. *Month. Notices R. Astron. Soc.* 390, 371–376. doi: 10.1111/j.1365-2966.2008.13753.x

Katarzyński, K., Sol, H., and Kus, A. (2001). The multifrequency emission of Mrk 501. From radio to TeV gamma-rays. *Astron. Astrophys.* 367, 809–825. doi: 10.1051/0004-6361:20000538

Landt, H., Ward, M. J., Baloković, M., Kynoch, D., Storchi-Bergmann, T., Boisson, C., et al. (2017). On the black hole mass of the γ-ray emitting narrow-line Seyfert 1 galaxy 1H 0323+342. *Month. Notices R. Astron. Soc.* 464, 2565–2576. doi: 10.1093/mnras/stw2447

Lenain, J.-P., Boisson, C., Sol, H., and Katarzyński, K. (2008). A synchrotron self-Compton scenario for the very high energy γ-ray emission of the radiogalaxy M 87. Unifying the TeV emission of blazars and other AGNs? *Astron. Astrophys.* 478, 111–120. doi: 10.1051/0004-6361:20077995

Paliya, V. S., Sahayanathan, S., Parker, M. L., Fabian, A. C., Stalin, C. S., Anjum, A., et al. (2014). The peculiar radio-loud narrow line seyfert 1 galaxy 1H 0323+342. *Astrophys. J.* 789:143. doi: 10.1088/0004-637X/789/2/143